AGU PUBLICATIONS

Geophysical Research Letters

RESEARCH LETTER
10.1002/2016GL071812

Key Points:
- Assimilation of TEC observations into a thermosphere-ionosphere model results in improved prereversal enhancement (PRE) *E* field modeling
- The improved PRE *E* field is achieved by assimilative adjustments of eastward neutral wind and associated gradients of conductivities
- Improved *E* field drives stronger plasma fountain at dusk creating equatorial trough and further strengthens the winds by ion drag reduction

Correspondence to:
C. Lin,
charles@mail.ncku.edu.tw

Citation:
Chen, C.-H., C. Lin, W.-H. Chen, and T. Matsuo (2017), Modeling the ionospheric prereversal enhancement by using coupled thermosphere-ionosphere data assimilation, *Geophys. Res. Lett.*, *44*, 1652–1659, doi:10.1002/2016GL071812.

Received 3 NOV 2016
Accepted 2 FEB 2017
Accepted article online 3 FEB 2017
Published online 25 FEB 2017

Modeling the ionospheric prereversal enhancement by using coupled thermosphere-ionosphere data assimilation

Chia-Hung Chen[1], Charles Lin[1], Wei-Han Chen[1], and Tomoko Matsuo[2,3]

[1]Department of Earth Sciences, National Cheng Kung University, Tainan, Taiwan, [2]Cooperative Institute for Research in Environmental Sciences, University of Colorado Boulder, Boulder, Colorado, USA, [3]Space Weather Prediction Center, National Oceanic and Atmospheric Administration, Boulder, Colorado, USA

Abstract We report that assimilating total electron content (TEC) into a coupled thermosphere-ionosphere model by using the ensemble Kalman filter results in improved specification and forecast of eastward prereversal enhancement (PRE) electric field (*E* field). Through data assimilation, the ionospheric plasma density, thermospheric winds, temperature, and compositions are adjusted simultaneously. The improvement of duskside PRE *E* field calculation over the prior state is achieved primarily by intensification of eastward neutral wind. The improved *E* field calculation promotes a stronger plasma fountain and deepens the equatorial trough. As a result, the horizontal gradients of Pedersen conductivity and eastward wind are increased due to greater zonal electron density gradient and smaller ion drag at dusk, respectively. Such modifications provide preferable conditions and obtain a strengthened PRE magnitude closer to the observation. The adjustment of PRE *E* field is enabled through self-consistent thermosphere and ionosphere coupling processes captured in the model. This study suggests that the PRE *E* field that is critical in driving the evening equatorial plasma instability could be better forecasted by assimilation of TECs in the 10 min cycling.

1. Introduction

The prereversal enhancement (PRE) of upward plasma ($E \times B$) drift near local sunset is an important feature in the low-latitude ionosphere and can uplift the height of the *F* region ionosphere in the equatorial region, which is important to generation of the postsunset *F* region plasma instability or plasma bubbles which interfere the radio communications. The features and the mechanism of PRE have been extensively investigated in the past. Suggested PRE formation mechanisms include the "edge effect" of vertical polarization charges at the terminator sector [*Rishbeth*, 1971], the *F* region dynamo by the horizontal conductivity gradients near sunset [*Heelis et al*., 1974], the rapid reduction of the *E* region Hall conductivity around sunset longitudes [*Farley et al*., 1986], and the zonal gradient and vertical shear of the zonal wind around evening [*Heelis*, 2004; *Fang*, 2009].

Recently, with the increased availability of observations from Global Navigation Satellite Systems, ionospheric data assimilation reduces the deviation between the modeled and observed electron densities and thus provides improvements in electron density calculation or forecast [*Schunk et al*., 2004]. A number of ionospheric data assimilation approaches have been developed, including the ones based on empirical models of the ionosphere [e.g., *Bust et al*., 2004; *Yue et al*., 2012; *Lin et al*., 2015], physics-based ionosphere models with specified thermospheric parameters [e.g., *Pi et al*., 2003, 2009; *Scherliess et al*., 2004; *Datta-Barua et al*., 2013], and physics-based coupled models of the ionosphere and thermosphere [e.g., *Matsuo and Araujo-Pradere*, 2011; *Lee et al*., 2012].

Physics-based models could reproduce observed PRE features, but they often require tuning of the corresponding model parameters by trial and error. For example, *Fesen et al*. [2000] showed that Thermosphere-Ionosphere-Electrodynamics General Circulation Model (TIEGCM) could not reproduce PRE when the *E* region electron density is greater than 10^4 cm^{-3}. Neutral wind effects are considered as an important factor that controls PRE formation and strength. *Fesen et al*. [2000] and *Millward et al*. [2001] both indicate that the specification of semidiurnal tides could affect the PRE modeling prominently. Recently, *Heelis et al*. [2012] and *Richmond et al*. [2015] have suggested the important role of eastward neutral wind at the *F* layer that drives ions to move with the winds, promoting their upward motion. The plasma convection vortex, eastward in the *F* layer, westward in the *E* layer, and upward around dusk, is adopted to give new insight into PRE formation. The purpose of this study is to demonstrate and examine the PRE modeling that is enabled by

assimilation of total electron content (TEC) observations into the TIEGCM during the geomagnetically quiescent period around equinox of 13–14 March 2015. The study's specific objectives are to investigate how the PRE features are reproduced during the forecast cycle of ensemble Kalman filtering through self-consistent thermosphere-ionosphere coupling processes captured in the TIEGCM and to interpret the PRE specification and forecast resulting from a coupled thermosphere-ionosphere data assimilation according to the latest theory of PRE formation.

2. Description of Data Assimilation Approach

The forecast model used in our assimilative system is a three-dimensional global numerical model (TIEGCM). The solar UV and EUV fluxes in this model are parameterized according to the solar $F_{10.7}$ daily index. The high-latitude ion convention pattern is obtained from the Heelis model [*Heelis et al*., 1982], and the electric fields at low latitude and midlatitude regions are calculated with the assumption of equal potential along the magnetic field line [*Richmond et al*., 1992]. An ensemble Kalman filter data assimilation system built with the Data Assimilation Research Testbed (DART) community software [*Anderson et al*., 2009] is employed to combine the TIEGCM and observations, called as DART/TIEGCM data assimilation system [*Lee et al*., 2012]. The 90-member ensemble of TIEGCM simulations is initialized by perturbing $F_{10.7}$ and *Kp* indices according to the centered Gaussian distributions with a standard deviation of ±20 ($10^{-22}\,\mathrm{Wm}^{-2}\,\mathrm{Hz}^{-1}$) and ±1 (geomagnetic quiet time *Kp*), respectively [cf. *Chen et al*., 2016]. During the entire DART/TIEGCM assimilation experiment, the $F_{10.7}$ and *Kp* indices are specified by the realistic values that change with time. The covariance estimated from the prior ensemble is tapered with the fifth-order piecewise rational function [*Gaspari and Cohn*, 1999] in order to eliminate effects of spurious correlation resulting from sampling errors at horizontal distance beyond 2000 km. The impact of different tapering length scales on the quality of assimilation analysis is discussed in detail by *Lee* [2013]. The unobserved model state variables (neutral temperature, atomic and molecular oxygen mixing ratios (O, O_2), neutral winds, and atomic oxygen ion density (O^+)) and electron density (*Ne*) are included in the state vector of the DART/TIEGCM. The observed ionospheric states and unobserved thermospheric states will be updated according to their respective correlative relationships to the TEC observations, as described in the earlier studies with the DART/TIEGCM [*Hsu et al*., 2014; *Chartier et al*., 2016; *Chen et al*., 2016].

The ground-based Global Positioning System (GPS) TEC observations are assimilated into the TIEGCM every 10 min. The TIEGCM solves the ionosphere-thermosphere coupled energy, momentum, and continuity equations with self-consistent electrodynamics. The overall spatial and temporal distributions of electrostatic potential (or *E* field) are determined in the TIEGCM's electrodynamics module by imposing the condition of a divergence free current system given neutral wind and conductivity distributions that are affected by the data assimilation process. Electrodynamic adjustment during the forecast cycle of ensemble Kalman filtering gives rise to strengthening of the PRE *E* field calculation under investigation.

In this study, two experiments were performed with updating all state vector variables (TEC, *Ne*, $[O^+]$, $[O_1]$, $[O_2]$, *Tn*, *Un*, and *Vn*) (experiment A) and without updating the neutral temperature (*Tn*) and neutral winds (*Un* and *Vn*) (experiment B). The purpose of experiment B is to evaluate the importance of neutral winds, which is considered as the main driver of PRE formation. Note that, in experiment B, although the unobserved state variables of neutral temperature and winds are not directly updated by the assimilation, changes of these parameters are still expected as they will be indirectly influenced by other updated variables along time steps.

3. Results and Discussions

Figure 1 displays the global TEC observations from globally 2127 ground-based GPS receivers (Figure 1a), TIEGCM default run (referred to as the control run henceforth; Figure 1d), and the DART/TIEGCM experiment results (Figures 1b, 1c, 1e, and 1f) at 1200 UT on 14 March 2015. In each 10 min cycle, around 16,980 observation points of vertical GPS-TEC are binned into a $1° \times 1°$ horizontal resolution for assimilation. Compared with the control run, the observations show a longer tail of equatorial ionization anomaly (EIA) over the geographic longitude of 90°E to 150°E (around 1800–2200 LT). After assimilating the GPS-TECs, both assimilation (posterior) and 10 min forecast (prior) results show clear separation of EIA crests and equatorial TEC trough. The well-separated EIA with the poleward extension is produced by the stronger plasma fountain effect

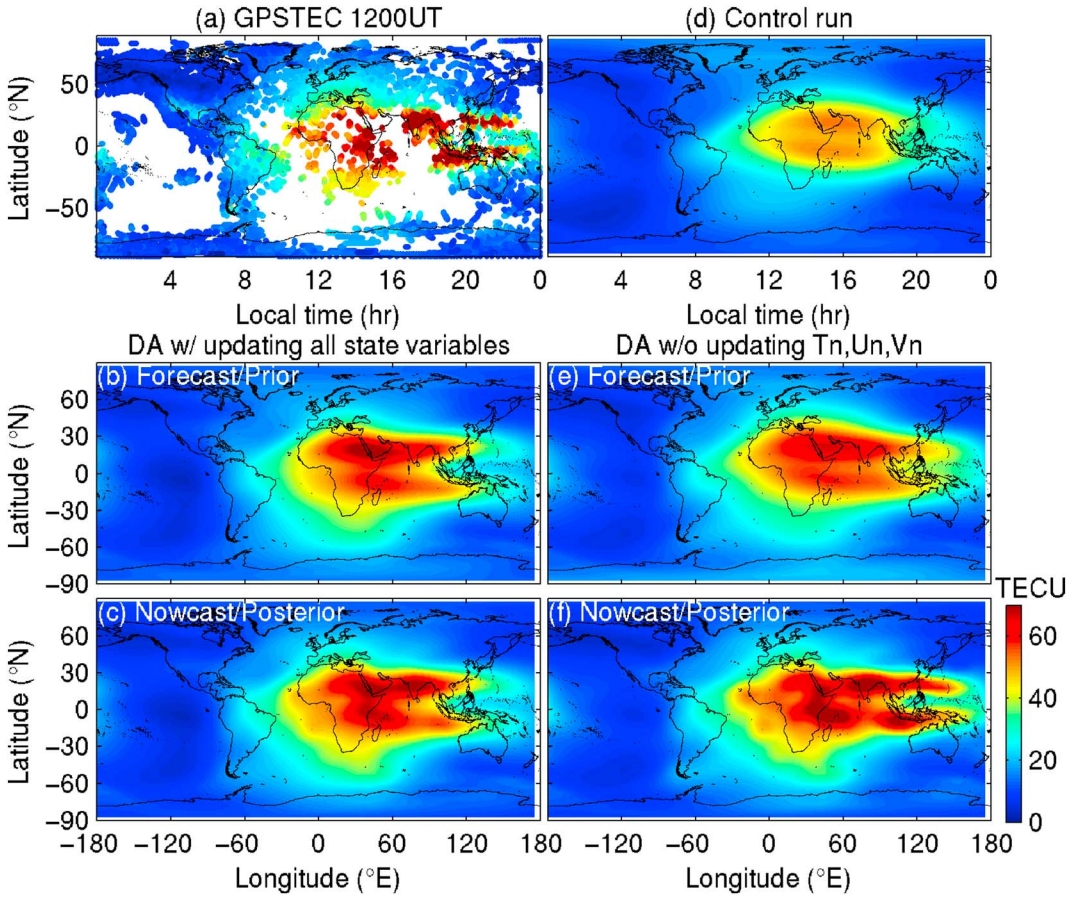

Figure 1. Global TEC distributions at 1200 UT on 14 March 2015. There are (a) GPS-TEC, (b) forecast, and (c) nowcast by assimilation model with updating all state variables and (d) default model/control run, (e) forecast, (f) and nowcast by assimilation model without updating the neutral temperature and neutral winds.

due to the stronger PRE. As the result of the stronger plasma fountain during postsunset, the equatorial trough becomes more prominent due to lack of photoionization after sunset. The horizontal gradient around the equatorial trough may contribute to PRE intensification by the greater gradient of conductivity along local times as well as the stronger neutral winds due to less ion drag. Figure 2 further illustrates the related global distribution of eastward *E* fields from the control run (Figure 2a), DART/TIEGCM experiment results (Figures 2b and 2d), and the differences (Figures 2c and 2e). The control run result shows that a weak eastward *E* field appears around the geographic latitude of 10°N (around geomagnetic equator) and longitude of 105°E (1900 LT). The eastward *E* field is further enhanced in experiment A at the location of TEC trough (Figures 2b and 2c). However, this enhancement is not obvious in experiment B (Figures 2d and 2e).

We compare the vertical drifts of DART/TIEGCM with the empirical model and the observations from Jicamarca Radio Observatory (JRO). Figure 3a presents the vertical $E \times B$ drift for the control (magenta), the assimilative results of experiments A (red) and B (green), and the output of Fejer-Scherliess model (black) [*Scherliess and Fejer*, 1999] in 13 March 2015 (local time) around JRO location. As JRO only has the observations available during 23–27 of the entire March 2015, more model runs of experiment A are performed during the period to compare the day-to-day results (red) with the JRO observations (blue) and the output of Fejer-Scherliess model (black) in Figure 3b. Figure 3a shows that the results from experiment A, including the neutral wind adjustment, greatly enhance the PRE magnitude, whereas experiment B has little effect to strengthen the PRE. This result indicates that assimilative adjustment of *Tn*, *Un*, and *Vn* is crucial for intensification of eastward PRE *E* field in our data assimilation system. It is noted that the PRE from experiment A is stronger than the Fejer-Scherliess model and there is an ~1 h late reversal of $E \times B$ drift (~2100 LT). The

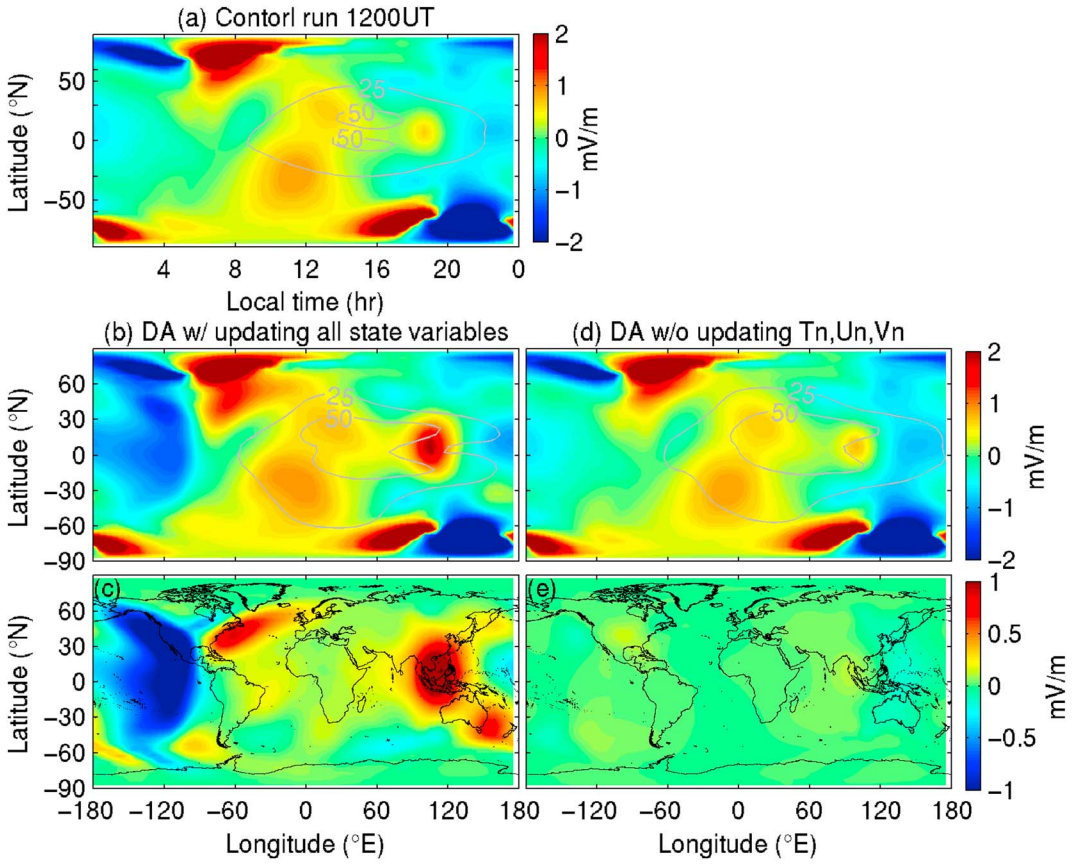

Figure 2. Global geographical eastward electric fields at 1200 UT on 14 March 2015. There are (a) default model/control run, forecast results by assimilation model (b) with updating all state variables and (d) without updating the neutral temperature and neutral winds, and differences between (c) forecast and (e) control run. The gray line indicates the isolated TEC contour line.

late reversal may be due to the weaker correlative relationship between the neutral winds and electron density at the *F* region of EIA around 2100 LT (figure not shown).

Figure 3b shows that the multiple day PRE vertical $E \times B$ drifts of experiment A are generally in good agreement with JRO observations, indicating the potential of strengthening PRE with the data assimilation system. The comparison, however, also shows some disagreements during the late evening and postmidnight sectors. The disagreement during the late evening may again result from the weaker correlative relationship between the neutral winds and electron density at *F* region around 2100 LT. The comparisons at postmidnight show that the downward $E \times B$ drifts become stronger than the observations, with the shape of trough (Figures 3a and 3b). Such feature is also shown in previous theoretical studies discussing the *E* and *F* region dynamo coupling [e.g., *Heelis et al*., 1974; *Eccles*, 1998; *Millward et al*., 2001; *Fang*, 2009]. The feature is shown in *Millward et al*. [2001] and *Fang* [2009] when considering the *E* or *F* region dynamo and coupled *E* and *F* region dynamo. In *Heelis et al*. [1974], the feature appears in the case considering coupled *E* and *F* region dynamo, but it is not shown for the case considering only *E* region dynamo. On the other hand, *Eccles* [1998] showed the feature with coupled *E* and *F* region dynamo, but it is not shown for the case considering only *F* region dynamo. The inconsistency from these studies indicates that it may be related to a more complex *E* and *F* region dynamo coupling that should be further investigated. In our assimilation system, this discrepancy may result from the weaker correlative relationship between the neutral wind and electron density at *E* region, since the correlative relationship at *F* region is strong in postmidnight (figures not shown).

Farley et al. [1986] considered that convergence of Hall conductivity/current is the main driver for PRE formation. *Fesen et al*. [2000] suggested that reduction of *E* region conductivity is important for TIEGCM to reproduce PRE. Later studies [e.g., *Heelis*, 2004; *Fang*, 2009] show that the *F* region dynamo is important in

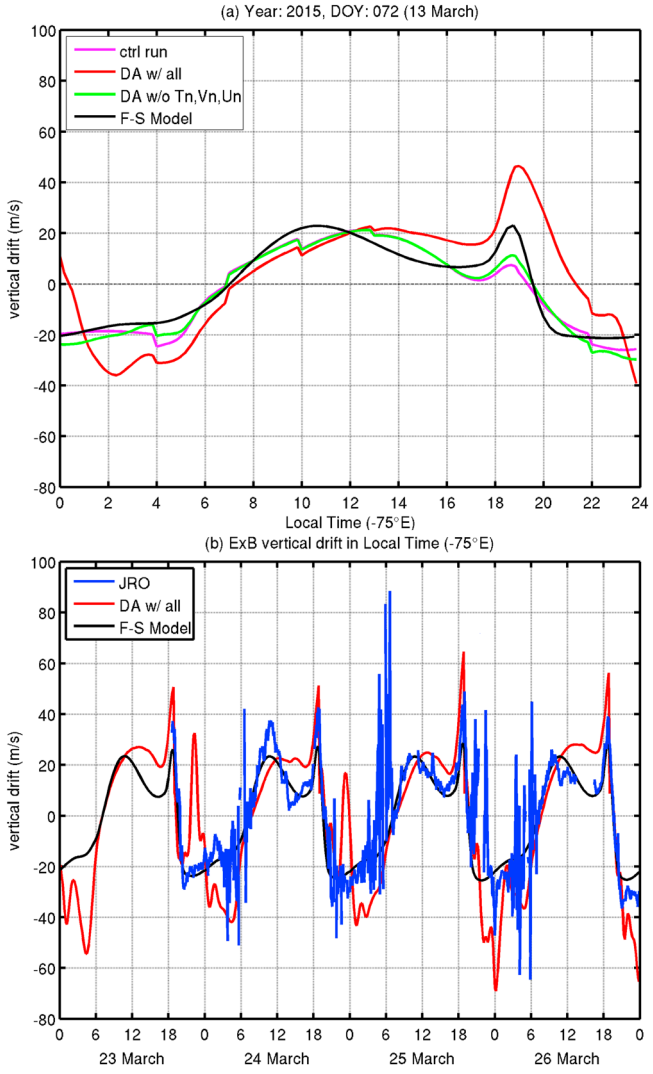

Figure 3. Local time variations of vertical drifts at −75°E on (a) 13 March 2015 and (b) 23–26 March 2015. There are default model/control run (pink line), assimilative ionosphere model (red and green lines), and the values of 13 March (Figure 3a) and 23–26 March (Figure 3b) output from the empirical model (black). The blue line is the vertical drift from Jicamarca Radio Observatory (JRO) on 13 March (Figure 3a) and 23–26 March (Figure 3b), which are the ionospheric quiet days.

driving the vertical Pedersen current for PRE. To examine the conductivity variations, we compare the zonal gradient of Pedersen (Figure 4) and Hall (not shown) conductivities around dusk longitudes from experiments A and B to the control run. The comparison shows that the zonal gradient of Pedersen conductivity increases much more for experiment A than B above 200 km altitude. The zonal gradients of Hall conductivity have the similar variations compared to the control run. Figure 5 further shows the eastward winds around dusk longitudes from the control and experiments A and B. The winds from experiment B (Figure 5c) are similar to the control run (Figure 5a) with some increases at the equatorial region of 100°E. The eastward winds for experiment A (Figure 5b) increase considerably above 200 km altitude at 100°E (1840 LT) and 110°E (1920 LT) longitudes for both equatorial and low-latitude regions, whereas the westward winds below 200 km are decreased. The results in Figures 4 and 5 show that assimilative adjustment of *Tn*, *Un*, and *Vn* affects not only the zonal winds but also the conductivities prominently.

Adjustment of PRE $E \times B$ drift was first reported in earlier assimilation work by *Pi et al*. [2003] by using a variational data assimilation approach. They demonstrate that the $E \times B$ vertical drift could be improved from "climatology" to "weather" for strong PRE by assimilating GPS-TEC data. In some recent studies, upward plasma drift is shown to be a part of the evening plasma convection vortex driven by the neutral wind and ion drag effects [e.g., *Kudeki and Bhattacharyya*, 1999; *Rodrigues et al*., 2012; *Heelis et al*., 2012; *Richmond et al*., 2015; *Richmond and Fang*, 2015]. The evening plasma vortex results from the eastward plasma flow at *F* layer height, the westward plasma flow in the *E* layer, and the vertical plasma flow that plays a role in balancing the zonal plasma shear. Thus, the stronger eastward plasma flow above and the weaker plasma flow below will promote the stronger vertical plasma flow, i.e., PRE of $E \times B$ vertical drift. The stronger eastward wind in the *F* layer and the weaker westward wind in the *E* layer adjusted by the assimilation (100 and 110°E in Figure 5b) in experiment A may drive stronger eastward plasma flow and weaker westward plasma flow, respectively. As described in *Richmond et al*. [2015], the stronger eastward *F* layer ion convection due to the stronger eastward wind at EIA region leads to PRE strengthening. On the other hand, eliminating the low-altitude westward wind is also found to PRE strengthening. Thus, the modified neutral winds in experiment A are in consistent with the theoretical results given by *Richmond et al*. [2015] and lead to the stronger modeled PRE (Figure 2b). In experiment B, without change of wind strength by the assimilation, although the conductivities are

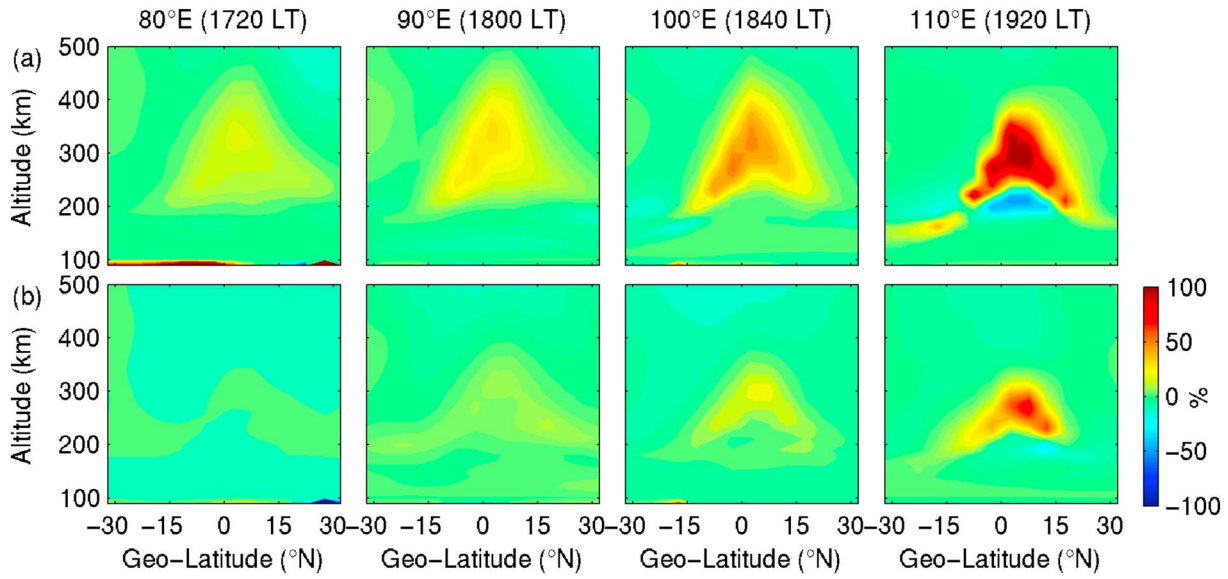

Figure 4. Latitudinal distribution of gradient Pedersen conductivity in different longitude sectors at 1200 UT on 14 March 2015. The result from the assimilation model (top) with updating all state variables and (bottom) without updating the neutral temperature and neutral winds. The color indicates the difference between the zonal gradient Pedersen conductivities of the assimilation and that of the control run. The calculation equation is $[\sigma_{Pf}(\text{longitude}-5°)-\sigma_{Pf}(\text{longitude}+5°)]/[\sigma_{Pf}(\text{longitude}-5°)+\sigma_{Pf}(\text{longitude}+5°)]\times 100\%-[\sigma_{Pc}(\text{longitude}-5°)-\sigma_{Pc}(\text{longitude}+5°)]/[\sigma_{Pc}(\text{longitude}-5°)+\sigma_{Pc}(\text{longitude}+5°)]$, while σ_{Pf} and σ_{Pc} indicate the Pedersen conductivities from the forecast and the control run, respectively. The "longitude" in the above equation is the same as the longitude at each panel title.

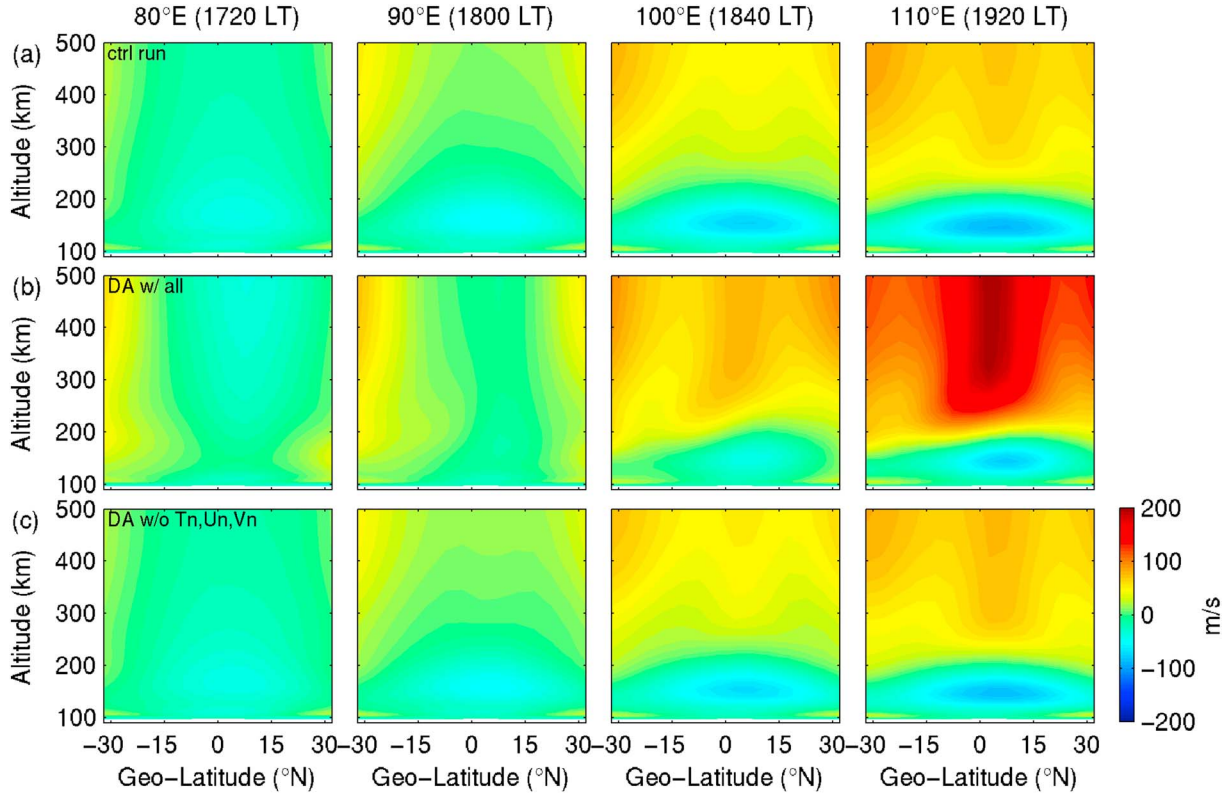

Figure 5. Latitudinal distribution of zonal (positive eastward) neutral wind in different longitude sectors at 1200 UT on 14 March 2015. (top) The default model/control run result. The result from the assimilation model (middle) with updating all state variables and (bottom) without updating the neutral temperature and neutral winds.

changed, the intensification of PRE is, however, small. Another important feature shown in Figure 5b is that the intensification of neutral winds occurs for both equatorial and low-latitude regions, since the eastward wind responsible to PRE intensification is mainly those at low-latitude EIA regions [*Richmond et al*., 2015].

Figure 5b indicates the considerably enhanced eastward neutral wind. It is also due to the stronger PRE leading to poleward extension of EIA crests around dusk and an electron density trough around the equator at dusk. The low electron density at the trough reduces the ion drag effect, and thus, the eastward wind is increased over time. This increased eastward wind has a positive impact on the PRE resulting in the separation of EIA crests, in agreement with the observations. In conclusion, the self-consistent thermosphere-ionosphere coupled assimilation system successfully improves the PRE modeling while adjusting model parameters in agreement with the latest theoretical explanation of PRE [*Heelis et al*., 2012; *Richmond et al*., 2015]. Through validations, the magnitude of PRE $E \times B$ drift from assimilation system is comparable to the observations, but with some discrepancies occurring after 2100 LT. Assimilation of neutral wind observations from ground-based Fabry-Perot interferometer or satellites may be helpful in future study.

Acknowledgments

This paper is supported by the Ministry of Science and Technology (MOST) and the National Space Organization (NSPO) of Taiwan to National Cheng Kung University under MOST-103-2111-M-006-003-MY3, 105-2111-M-006-003, 105-2111-M-006-008, 105-2119-M-006-025, and NSPO-S-105120. T.M. is supported by NASA award NNX14AI17G and AFOSR award FA9550-13-1-0058. The source code for the assimilation system and the simulation model used in this study, the DART and TIEGCM, are available at http://www.image.ucar.edu/DAReS/DART/ and http://www.hao.ucar.edu/modeling/tgcm/, respectively. The observation data from ground-based GPS receivers are available at IGS (https://igscb.jpl.nasa.gov/components/data.html). The authors are grateful for the NCAR High Altitude Observatory and Data Assimilation Research Section for their support of TIEGCM and DART software. The authors gratefully acknowledge the constructive comments given by the two anonymous reviewers. Charles Lin thanks Arthur D. Richmond for the useful discussion on the updated mechanisms of prereversal enhancement during the manuscript preparations.

References

Anderson, J. L., T. Hoar, K. Raeder, H. Liu, N. Collins, R. Torn, and A. F. Arellano (2009), The Data Assimilation Research Testbed: A community data assimilation facility, *Bull. Am. Meteorol. Soc.*, *90*, 1283–1296, doi:10.1175/2009BAMS2618.1.

Bust, G. S., T. W. Garner, and T. L. Gaussiran II (2004), Ionospheric data assimilation three-dimensional (IDA3D): A global, multi-sensor, electron density specification algorithm, *J. Geophys. Res.*, *109*, A11312, doi:10.1029/2003JA010234.

Chartier, A. T., T. Matsuo, J. L. Anderson, N. Collins, T. J. Hoar, G. Lu, C. N. Mitchell, A. J. Coster, L. J. Paxton, and G. S. Bust (2016), Ionospheric data assimilation and forecasting during storms, *J. Geophys. Res. Space Physics*, *121*, 764–778, doi:10.1002/2014JA020799.

Chen, C. H., C. H. Lin, T. Matsuo, W. H. Chen, I. T. Lee, J. Y. Liu, J. T. Lin, and C. T. Hsu (2016), Ionospheric data assimilation with Thermosphere-Ionosphere-Electrodynamics General Circulation Model and GPS-TEC during geomagnetic storm conditions, *J. Geophys. Res. Space Physics*, *121*, 5708–5722, doi:10.1002/2015JA021787.

Datta-Barua, S., G. S. Bust, and G. Crowley (2013), First storm time plasma velocity estimates from high-resolution ionospheric data assimilation, *J. Geophys. Res. Space Physics*, *118*, 7458–7471, doi:10.1002/2013JA019153.

Eccles, J. V. (1998), Modeling investigation of the evening prereversal enhancement of the zonal electric field in the equatorial ionosphere, *J. Geophys. Res.*, *103*, 26,709–26,719, doi:10.1029/98JA02656.

Fang, T.-W. (2009), Model simulation of the low-latitude ionosphere chap. 5, PhD thesis, Institute of Space Science, National Central Univ., Zhongli, Taoyuan, Taiwan.

Farley, D. T., E. Bonelli, B. G. Fejer, and M. F. Larsen (1986), The prereversal enhancement of the zonal electric field in the equatorial ionosphere, *J. Geophys. Res.*, *91*(A12), 13,723–13,728, doi:10.1029/JA091iA12p13723.

Fesen, C. G., G. Crowley, R. G. Roble, A. D. Richmond, and B. G. Fejer (2000), Simulation of the pre-reversal enhancement in the low latitude vertical ion drifts, *Geophys. Res. Lett.*, *27*(13), 1851–1854, doi:10.1029/2000GL000061.

Gaspari, G., and S. E. Cohn (1999), Construction of correlation functions in two and three dimensions, *Q. J. R. Meteorol. Soc.*, *125*, 723–757, doi:10.1002/qj.49712555417.

Heelis, R. A. (2004), Electrodynamics in the low and middle latitude ionosphere: A tutorial, *J. Atmos. Sol. Terr. Phys.*, *66*, 825–838.

Heelis, R. A., P. C. Kendall, R. J. Moffett, D. W. Windle, and H. Rishbeth (1974), Electrical coupling of the *E*- and *F*-regions and its effect of *F*-region drifts and winds, *Planet. Space Sci.*, *22*, 743–756.

Heelis, R. A., J. K. Lowell, and R. W. Spiro (1982), A model of the high latitude ionosphere convection pattern, *J. Geophys. Res.*, *87*, 6339–6345, doi:10.1029/JA087iA08p06339.

Heelis, R. A., G. Crowley, F. Rodrigues, A. Reynolds, R. Wilder, I. Azeem, and A. Maute (2012), The role of zonal winds in the production of a pre-reversal enhancement in the vertical ion drift in the low latitude ionosphere, *J. Geophys. Res.*, *117*, A08308, doi:10.1029/2012JA017547.

Hsu, C.-T., T. Matsuo, W. Wang, and J.-Y. Liu (2014), Effects of inferring unobserved thermospheric and ionospheric state variables by using an ensemble Kalman filter on global ionospheric specification and forecasting, *J. Geophys. Res. Space Physics*, *119*, 9256–9267, doi:10.1002/2014JA020390.

Kudeki, E., and S. Bhattacharyya (1999), Postsunset vortex in equatorial *F*-region plasma drifts and implications for bottomside spread-*F*, *J. Geophys. Res.*, *104*, 28,163–28,170, doi:10.1029/1998JA900111.

Lee, I. T. (2013), Assimilation of radio occultation data observed by FORMOSAT-3/COSMIC into a coupled thermosphere/ionosphere model chap. 2, PhD thesis, Institute of Space Science, National Central Univ., Zhongli, Taoyuan, Taiwan.

Lee, I. T., T. Matsuo, A. D. Richmond, J. Y. Liu, W. Wang, C. H. Lin, J. L. Anderson, and M. Q. Chen (2012), Assimilation of FORMOSAT-3/COSMIC electron density profiles into a coupled thermosphere/ionosphere model using ensemble Kalman filtering, *J. Geophys. Res.*, *117*, A10318, doi:10.1029/2012JA017700.

Lin, C. Y., T. Matsuo, J. Y. Liu, C. H. Lin, H. F. Tsai, and E. A. Araujo-Pradere (2015), Ionospheric assimilation of radio occultation and ground-based GPS data using non-stationary background model error covariance, *Atmos. Meas. Tech.*, *8*, 171–182.

Matsuo, T., and E. A. Araujo-Pradere (2011), Role of thermosphere-ionosphere coupling in a global ionospheric specification, *Radio Sci.*, *46*, RS0D23, doi:10.1029/2010RS004576.

Millward, G. H., I. C. F. Müller-Wodarg, A. D. Aylward, T. J. Fuller-Rowell, A. D. Richmond, and R. J. Moffett (2001), An investigation into the influence of tidal forcing on *F* region equatorial vertical ion drift using a global ionosphere-thermosphere model with coupled electrodynamics, *J. Geophys. Res.*, *106*(A11), 24,733–24,744, doi:10.1029/2000JA000342.

Pi, X., C. Wang, G. A. Hajj, G. Rosen, B. D. Wilson, and G. J. Bailey (2003), Estimation of $E \times B$ drift using a global assimilative ionospheric model: An observation system simulation experiment, *J. Geophys. Res.*, *108*(A2), 1075, doi:10.1029/2001JA009235.

Pi, X., A. J. Mannucci, B. A. Iijima, B. D. Wilson, A. Komjathy, T. F. Runge, and V. Akopian (2009), Assimilative modeling of ionospheric disturbances with FORMOSAT-3/COSMIC and ground-based GPS measurements, *Terr. Atmos. Ocean. Sci.*, *20*(1), 273–285.

Richmond, A. D., and T.-W. Fang (2015), Electrodynamics of the equatorial evening ionosphere: 2. Conductivity influences on convection, current, and electrodynamic energy flow, *J. Geophys. Res. Space Physics*, *120*, 2133–2147, doi:10.1002/2014JA020935.

Richmond, A. D., E. C. Ridley, and R. G. Roble (1992), A Thermosphere/Ionosphere General Circulation Model with coupled electrodynamics, *Geophys. Res. Lett.*, *19*(6), 601–604, doi:10.1029/92GL00401.

Richmond, A. D., T.-W. Fang, and A. Maute (2015), Electrodynamics of the equatorial evening ionosphere: 1. Importance of winds in different regions, *J. Geophys. Res. Space Physics*, *120*, 2118–2132, doi:10.1002/2014JA020934.

Rishbeth, H. (1971), The *F*-layer dynamo, *Planet. Space Sci.*, *19*, 263–267, doi:10.1016/0032-0633(71)90205-4.

Rodrigues, F. S., G. Crowley, R. A. Heelis, A. Maute, and A. Reynolds (2012), On TIE-GCM simulation of the evening equatorial plasma vortex, *J. Geophys. Res.*, *117*, A05307, doi:10.1029/2011JA017369.

Scherliess, L., and B. G. Fejer (1999), Radar and satellite global equatorial *F* region vertical drift model, *J. Geophys. Res.*, *104*(A4), 6829–6842, doi:10.1029/1999JA900025.

Scherliess, L., R. W. Schunk, J. J. Sojka, and D. C. Thompson (2004), Development of a physics-based reduced state Kalman filter for the ionosphere, *Radio Sci.*, *39*, RS1S04, doi:10.1029/2002RS002797.

Schunk, R. W., et al. (2004), Global Assimilation of Ionospheric Measurements (GAIM), *Radio Sci.*, *39*, RS1S02, doi:10.1029/2002RS002794.

Yue, X., et al. (2012), Global 3-D ionospheric electron density reanalysis based on multisource data assimilation, *J. Geophys. Res.*, *117*, A09325, doi:10.1029/2012JA017968.